energies

MDPI

Article

Thermo-Economic Analysis on Integrated CO_2, Organic Rankine Cycles, and NaClO Plant Using Liquefied Natural Gas

Tri Tjahjono [1], Mehdi Ali Ehyaei [2,*], Abolfazl Ahmadi [3], Siamak Hoseinzadeh [4,*] and Saim Memon [5,*]

[1] Department of Mechanical Engineering, Universitas Muhammadiyah Surakarta, Surakarta 57102, Indonesia; tt142@ums.ac.id
[2] Department of Mechanical Engineering, Pardis Branch, Islamic Azad University, Pardis New City 1468995513, Iran
[3] Department of Energy Systems Engineering, School of Advanced Technologies, Iran University of Science and Technology, Tehran 13114-16846, Iran; a_ahmadi@iust.ac.ir
[4] Department of Planning, Design, and Technology of Architecture, Sapienza University of Rome, Piazzale Aldo Moro 5, 00185 Roma, Italy
[5] Solar Thermal Vacuum Engineering Research Group, London Centre for Energy Engineering, School of Engineering, London South Bank University, London SE1 0AA, UK
* Correspondence: aliehyaei@pardisiau.ac.ir (M.A.E.); siamak.hosseinzadeh@uniroma1.it (S.H.); S.Memon@lsbu.ac.uk (S.M.); Tel.: +0044-20-7815-7510 (S.M.)

Abstract: The thermal energy conversion of natural gas (NG) using appropriate configuration cycles represents one of the best nonrenewable energy resources because of its high heating value and low environmental effects. The natural gas can be converted to liquefied natural gas (LNG), via the liquefaction process, which is used as a heat source and sink in various multigeneration cycles. In this paper, a new configuration cycle is proposed using LNG as a heat source and heat sink. This new proposed cycle includes the CO_2 cycle, the organic Rankine cycle (ORC), a heater, a cooler, an NaClO plant, and reverse osmosis. This cycle generates electrical power, heating and cooling energy, potable water (PW), hydrogen, and salt all at the same time. For this purpose, one computer program is provided in an engineering equation solver for energy, exergy, and thermo-economic analyses. The results for each subsystem are validated by previous researches in this field. This system produces 10.53 GWh electrical energy, 276.4 GWh cooling energy, 1783 GWh heating energy, 17,280 m^3 potable water, 739.56 tons of hydrogen, and 383.78 tons of salt in a year. The proposed system energy efficiency is 54.3%, while the exergy efficiency is equal to 13.1%. The economic evaluation showed that the payback period, the simple payback period, the net present value, and internal rate of return are equal to 7.9 years, 6.9 years, 908.9 million USD, and 0.138, respectively.

Keywords: energy; exergy; thermo-economic; CO_2 cycle; organic Rankine cycle; reverse osmosis

Citation: Tjahjono, T.; Ehyaei, M.A.; Ahmadi, A.; Hoseinzadeh, S.; Memon, S. Thermo-Economic Analysis on Integrated CO2, Organic Rankine Cycles, and NaClO Plant Using Liquefied Natural Gas. Energies**2021**, *14*, 2849. https://doi.org/10.3390/en14102849

Academic Editor: Carlo Renno

Received: 14 April 2021
Accepted: 13 May 2021
Published: 14 May 2021

1. Introduction

Energy demand is envisaged to increase by approximately 50% by 2070 [1]. Whilst renewable energy sources are exponentially growing, the stable high-power generation of nonrenewable methods is still required for industrialization. Due to the shortage and the environmental impacts of nonrenewable energy resources, the development of new methods of energy utilization is necessary [2]. For achieving this target, the use of natural gas (NG) is a prime candidate due to its high lower heating value (LHV), high H/C ratio (hydrogen/carbon), and low environmental pollution, making it the cleanest fossil fuel [3,4]. For easier transportation and storage, NG liquefaction is an appropriate approach, especially for remote regions.

LNG is a liquid state of natural gas which has a maximum amount of methane (CH_4), with other components such as ethane (C_2H_6) and propane (C_3H_8). This mixture is cooled to below 113.1 K, changing its state from gas to liquid through a cryogenic process,

thereby facilitating shipping and storage. The volume of LNG is 600 times smaller than that of natural gas. Upon reaching its destination, LNG is reverted to natural gas and distributed via pipelines to the final consumers, comprising industries, residential buildings, and commercial buildings [5].

Today, LNG can be used in a variety of ways, e.g., air separation [6,7], food freezing [8], potable water production [9], air conditioning [10,11], petrochemical power production [12,13], and electrical power production [14].

LNG can be used for electrical power production as a heat source or sink. For heat source applications, it can be used as fuel upon conversion to NG. Moreover, it can be used as a heat sink to absorb the cycle's heat dissipation via a condenser [15].

Most thermodynamic cycles can use LNG, such as the direct expansion cycle (DEC) [16], organic Rankine cycle (ORC) [17,18], Kalina cycle [19], Brayton cycle [20,21], combined cycle [22], and CO_2 cycle [23].

Literature Review

The thermodynamic performance of the hybrid integration of a two-stage ORC with R116 and R227ea as the working fluid, driven by low-grade heat and LNG as the cryogenic energy storage, was studied. The results of this study stated that a two-stage ORC system was able to produce 1776.44 kW of power with 25.64% thermal efficiency and 31.02% exergy efficiency. Moreover, the cost of power production for this system was 6.3 USD/W, since the LNG temperature was about 283.15 K [24].

The CO_2 cryogenic flue gas capture of an LNG power generation system was investigated. In this system, the flue gas was compressed to remove CO_2 from the exhaust gas. The results of this study showed that this system could obtain a 90% CO_2 recovery rate [25].

The performance of a combined gas system coupled with cold energy released during the regasification process of LNG was investigated. The results showed that the electrical efficiency of this system could be increased by about 8% [26].

The performance of an advanced thermal power plant was compared with a conventional combined power plant. In this comparison, the usage of intercooling and inlet air cooling was investigated. Furthermore, the latent heat of steam from a steam turbine and the heat rejected from compressed air were used for power generation and to heat the LNG. The results showed that the overall output work and electrical efficiency of the combined cycle increased by 2.8% up to 76.8 MW [27,28].

An ammonia/water-based combined power cooling cycle with LNG as cold storage, driven by low-temperature waste heat, was employed for electrical generation and as a district cooling system in coastal hot climate regions. At 70 °C heat source temperature, the system's energy efficiency was 39% and the system's exergy efficiency was 36% [29].

A novel system comprising a combination of biomass-based gas and steam cycles, a cascade ORC, an absorption refrigeration system, a PEM fuel cell, and LNG as a thermal sink was applied for power, cooling, and hydrogen production. The results showed that the mass flow rate of the fuel was the most important factor affecting the energy efficiency and the total cost. As a result, an increase of 4 $kg \cdot s^{-1}$ to 10 $kg \cdot s^{-1}$ in the mass flow rate of the fuel caused a decrease of 8.5% in the total cost and an increase of 122.8% in the system's energy efficiency [30].

A mathematical model for the integration of a solid oxide fuel cell, gas and CO_2 cycles, and ORC using LNG cold energy storage was applied to achieve cascade energy exploitation and CO_2 capture. The results showed that an energy efficiency of 79.48% and an exergy efficiency of 62.3% were obtained [31].

A summary of the studies related to LNG-powered multigeneration systems is presented in Table 1.

Table 1. Studies related to multigeneration systems.

No.	Energy Resource	LNG		Components	Products	Results	Ref
		Heat Source	Heat Sink				
1	Solar		●	CO_2 cycle, FPC, RO, NaClO plant, Stirling engine	Electrical, NaCl, hydrogen, PW	The exergy destruction rate was decreased from 16.7% to 8.8% upon replacement of the condenser by a Stirling engine	[32]
2	Solar		●	Transcritical CO_2 cycle, FPC, RO, NaClO plant	Electrical, NaCl, hydrogen, PW	The system net output power was increased by increasing the inlet temperature of the boiler and turbine	
3	Geothermal		●	CO_2 cycle	Electrical	The system exergy efficiency was equal to 20.5% The product cost rate was equal to 263,592.15 USD/year	[14]
4	Exhaust hot gas of combined cycle		●	Two-stage ORC	Electrical	The energy and exergy efficiencies were 25.64% and 31.02% CPP was equal to 6.3 USD/W	
5	LNG	●		RC, ASU, LAES	Electrical, clean air	The maximum amount of net output power ranged from 85.7–94.8 kJ/kgLNG	[23]
6	LNG	●		ASU, GC, CO_2 capture	Electrical, CO_2	90% CO_2 recovery	
7	NG		●	RC, direct expander	Electrical	The maximum exergy efficiency was obtained by 302.8 kJ/kg LNG	[24]
8	LNG	●	●	CCGT, LNG regasification process	Electrical	The electrical efficiency was increased from 6.32% to 9.09%	
9	LNG	●	●	CCPP, IAC, intercooling	Electrical	The electrical efficiency was improved by 2.8%	[15]
10	LNG	●	●	CCPP	Electrical	This system produced 3.36 MW and 21 MW of electrical power and cooling	
11	Geothermal		●	Absorption power/cooling cycle	Electrical	The system energy and exergy efficiencies were equal to 39% and 36%, respectively	[25]
12	Biomass		●	ARS, GC, RC, ORC, PEM Elec	Electrical, cooling, and hydrogen	Upon increasing the fuel mass flow rate from 4 to 10 kg/s, the system energy efficiency decreased by 8.5% and the cost rate increased by 122.8%	
13	LNG	●	●	SOFC, GC, CO_2 cycle, ORC, CO_2 capture	Electrical, cooling, heating, and CO_2	The system exergy efficiency was equal to 62.3%	[33]

14	Exhaust gas	•	KC, ORC, CO_2 capture	Electrical, CO_2	The system energy efficiency was equal to 36% The system exergy efficiency was equal to 41.4% The net electrical power output was equal to 394,658 kW	
15	Ambient air	•	CO_2 Rankine cycle	Electrical	The system thermal efficiency was equal to 6.75% The net output power was 108.7 kW	[26]

The novelty of this study, with respect to the references discussed in Table 1, is the investigation of a system that includes the ORC, the CO_2 cycle, RO, and an NaClO plant using LNG as a heat source and sink. Furthermore, the proposed cycle has various products, i.e., electrical power, heating and cooling, potable water (PW), hydrogen, and sodium chloride (NaCl), which are produced simultaneously when the system operates.

In this paper, integration of the CO_2 cycle and ORC is proposed using LNG as a heat source and heat sink. The LNG absorbs the dissipated heat of condensers of both cycles (heat sink). Then, it expands in turbine III for electrical production. Moreover, it is used in the cooler for cooling load production. At this stage, the LNG is converted to NG, and it reacts with air in the boiler to warm the water and convert it to steam. The produced steam is used in the steam generator and evaporator of the CO_2 cycle and ORC to meet the heat needs of both cycles. Additionally, it produces heating load in the heater. Some of the electrical power in both cycles is consumed in the RO and NaClO plants to simultaneously produce potable water (PW), hydrogen, and NaCl.

The novelties of this paper are as follows:

- A new multigeneration system is proposed using LNG as a heat source and sink;
- Energy, exergy, and economic investigations of the new configuration system are carried out;
- Various products are generated, i.e., electrical power, heating and cooling loads, PW, hydrogen, and NaCl.

2. Materials and Methods

Figure 1 shows a schematic diagram of the cycle. The working fluids in the CO_2 cycle and the organic Rankine cycle are carbon dioxide and R134a, respectively. The physical and thermodynamic properties of tetrafluoroethene (R134a) are similar to R12 with lower ozone depletion. This cycle is powered by LNG. Furthermore, the LNG is used as a heat sink. The LNG, after pressurizing in pump I (points 5, 6), absorbs the dissipated heat from the condensers of the CO_2 cycle and ORC (points 6, 7, 8). Then, it is expanded in turbine III and the generator to produce electricity (points 8, 9), while it is used as a coolant fluid in the cooler (points 9, 10), where it is also converted to NG (point 10). The NG is burned in the boiler to warm the water and convert it to steam (points 16, 17). The steam provides the heat for the steam generator (CO_2 cycle) and the evaporator of the ORC (points 17, 18, 36, 37). Some of the steam is used in the heater to produce heating energy (points 19, 20). The exhaust hot water of the ORC evaporator and heater is mixed, and it is transferred and pressurized in pump IV (points 15, 16, 20, 37). Some of the electricity produced in this system is consumed in the RO system to produce PW. In the RO system, seawater goes throughout pumps V and VI, and it is pressurized (points 21, 22, 23, 24, 25). The pressurized seawater is transferred to membranes I and II, and it is separated into brain water (points 27, 29) and potable water (points 26, 28, 30, 31). The brain water rotates the recovery turbine to recover energy and produce electrical power. Then, it is transferred to the NaClO plant, where it produces NaCl and hydrogen.

In the CO_2 cycle, the working fluid (CO_2) is pressurized in pump II (points 1, 2). Then, it exchanges energy with steam in a steam generator (points 2, 3, 17, 18), becoming superheated steam (point 3). Turbine I and the generator are operated by this superheated steam to produce electricity (points 3, 4). The turbine's exhaust steam changes to liquid by dissipating heat to LNG (points 1, 4, 6, 7). In the ORC, the working fluid (R134a) is pressurized in pump III (points 11, 12). The pressurized working fluid exchanges heat with steam in the evaporator (points 12, 13, 36, 37). Turbine II is rotated by the superheated steam (points 13, 14). Then, the working fluid transfers heat to LNG (points 7, 8, 11, 14).

In summary, in this cycle, four components produce electricity (turbines I, II, III, and the recovery turbine), while six components (pumps I to VI) and the NaClO plant consume electricity. Figure 2 shows the energy flow between the subsystems of the proposed system.

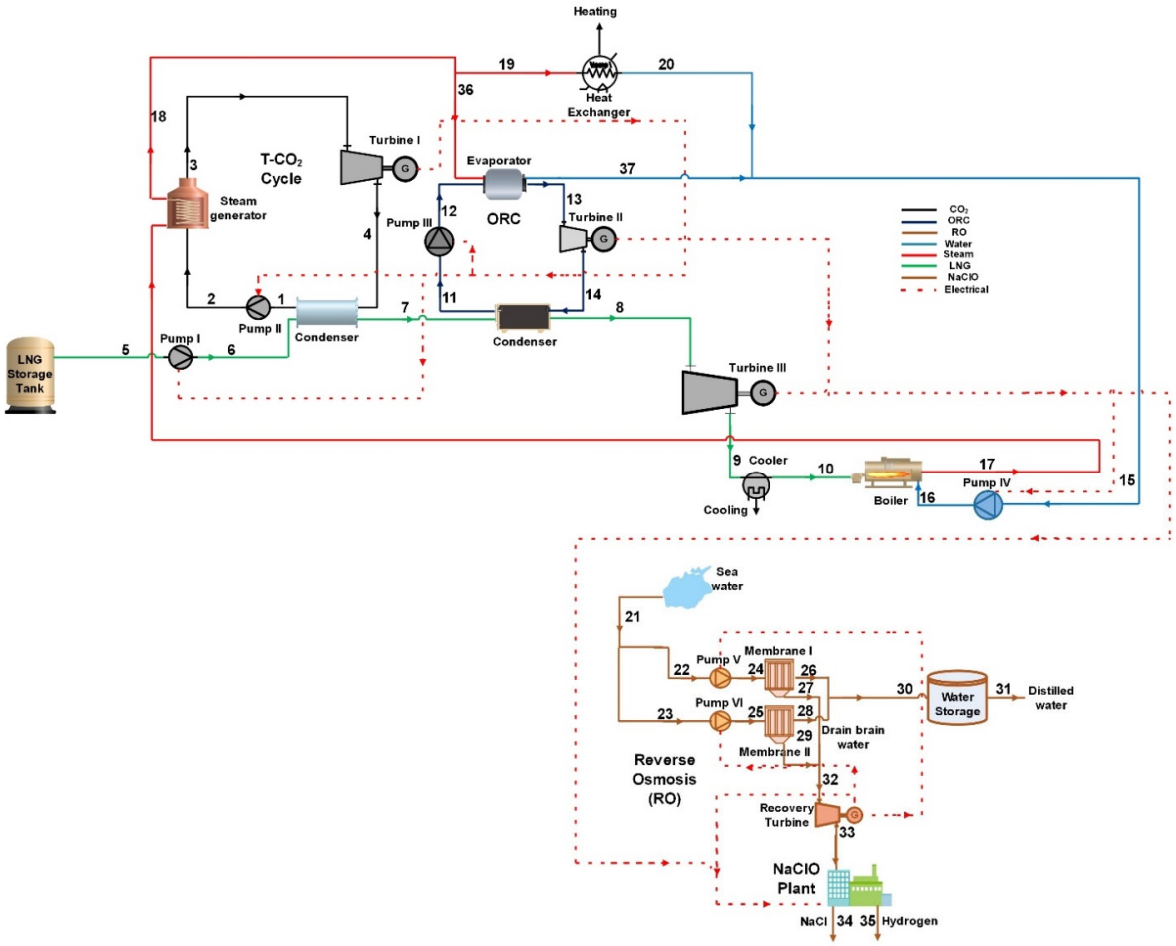

Figure 1. Schematic diagram of the system.

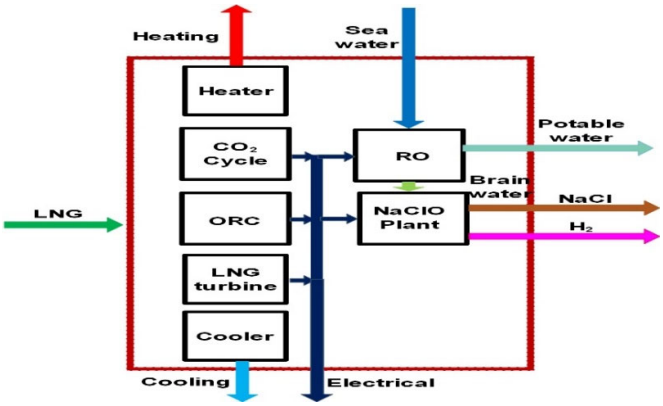

Figure 2. Energy flow between the subsystems.

The following assumptions are made in this study [14,21,32–34]:

(a) The system works in steady-state conditions;
(b) The ambient pressure and temperature are 288 K and 1 bar, respectively;
(c) Pressure loss in the heat exchanger is assumed to be 2%;
(d) The kinetic and potential energies are ignored;
(e) The pressure loss in the cycles is ignored;
(f) The turbine and pump polythrophic efficiencies are assumed to be 80%;
(g) The heat exchanger effectiveness factor is assumed to be 80%;
(h) The salt concentration in the electrolyzer is assumed constant;
(i) The inlet CO_2 and LNG of the pump are in a liquid state;
(j) The RO recovery ratio is 0.3.

2.1. Mathematical Modeling Approach

2.1.1. Mass and energy balance

In general, the mass and energy balance equations are described as shown below [35].

$$\sum_{in} \dot{m} = \sum_{out} \dot{m}, \tag{1}$$

$$\dot{Q} - \dot{W} = \sum_{P} \dot{m}\left(h_f + \left(h - h_0\right)\right) - \sum_{R} \dot{m}\left(h_f + (h - h_0)\right), \tag{2}$$

where $\dot{W}$ and $\dot{Q}$ are the power and heat transfer rate, while ṁ and h are the mass flow rate and enthalpy, respectively. Subscripts *R*, *f*, *P*, and *0* denote reactant, formation, product, and dead state, respectively.

The mass and energy balance relationships for the CO_2 cycle, ORC, LNG and water loops, and boiler are shown in Table 2 [23,36,37].

Table 2. Mass and energy balance relationships for the CO_2 cycle, ORC, LNG and water loops, and boiler.

No.	Components	Mass Balance	Energy Equation
		CO_2 cycle	
1	Pump II (P)	$\dot{m}_1 = \dot{m}_2$	$\dot{w}_{pII} = \dot{m}_1(h_2 - h_1)$
2	Steam generator	$\dot{m}_2 = \dot{m}_3, \dot{m}_{17} = \dot{m}_{18}$	$\dot{m}_2(h_3 - h_2) = \eta_{HX}\dot{m}_{17}(h_{17} - h_{18})$
3	Turbine I (T)	$\dot{m}_3 = \dot{m}_4$	$\dot{w}_{TI} = \dot{m}_3(h_3 - h_4)$
4	Condenser	$\dot{m}_4 = \dot{m}_1, \dot{m}_6 = \dot{m}_7$	$\dot{m}_7(h_7 - h_6)\eta_{HX} = \dot{m}_1(h_4 - h_1)$
		ORC	
5	Pump III (P)	$\dot{m}_{11} = \dot{m}_{12}$	$\dot{w}_{pIII} = \dot{m}_1(h_2 - h_1)$
6	Steam generator	$\dot{m}_{12} = \dot{m}_{13}, \dot{m}_{36} = \dot{m}_{37}$	$\dot{m}_{12}(h_{13} - h_{12}) = \eta_{HX}\dot{m}_{36}(h_{36} - h_{37})$

7	Turbine II (T)	$\dot{m}_{13} = \dot{m}_{14}$	$\dot{w}_{TII} = \dot{m}_{13}(h_{13} - h_{14})$
8	Condenser	$\dot{m}_{14} = \dot{m}_{11}, \dot{m}_7 = \dot{m}_8$	$\dot{m}_7(h_8 - h_7)\eta_{HX} = \dot{m}_{11}(h_{14} - h_{11})$
		LNG loop	
9	Pump I (P)	$\dot{m}_5 = \dot{m}_6$	$\dot{w}_{pI} = \dot{m}_5(h_6 - h_5)$
10	Turbine III (T)	$\dot{m}_8 = \dot{m}_9$	$\dot{w}_{TIII} = \dot{m}_8(h_8 - h_9)$
11	Cooler	$\dot{m}_9 = \dot{m}_{10}$	$\dot{Q}_{cooler} = \eta_{HX}\dot{m}_9(h_{10} - h_9)$
		Boiler	
12	Boiler	$\dot{m}_{17} = \dot{m}_{18}$	$\eta_{CC}\dot{m}_{10}LHV = \dot{m}_{16}(h_{17} - h_{16})$
		Water loop	
13	Pump IV (P)	$\dot{m}_{15} = \dot{m}_{16}$	$\dot{w}_{pIV} = \dot{m}_{15}(h_{16} - h_{15})$
14	Heater	$\dot{m}_{19} = \dot{m}_{20}$	$\dot{Q}_{heater} = \eta_{HX}\dot{m}_{19}(h_{19} - h_{20})$

The mass balance equations in the RO system are shown below [14,38,39].

$$\dot{m}_{SW} = \dot{m}_{BW} + \dot{m}_{PW}, \tag{3}$$

$$\dot{m}_{SW}x_{SW} = \dot{m}_{PW}x_{PW} + \dot{m}_{Bw}x_{BW}, \tag{4}$$

where x is the salt concentration. Subscripts *PW*, *SW*, and *BW* denote potable water, sea-water, and brain water, respectively.

The sea and potable water relationship is shown below [14,38].

$$\dot{m}_{PW} = RR\dot{m}_{SW}, \tag{5}$$

where *RR* denotes the recovery ratio.

The osmosis pressure for the sea, potable, and brain water streams is shown below [14,38].

$$\pi_{SW} = RuTx_{SW}, \tag{6}$$

$$\pi_{PW} = RuTx_{PW}, \tag{7}$$

$$\pi_{BW} = RuTx_{BW}, \tag{8}$$

where R defines the universal gas constant.

The membrane net pressure equation is shown below [14,38].

$$\Delta\pi = \left(\frac{\pi_{SW} + \pi_{BW}}{2}\right) - \pi_{PW}. \tag{9}$$

The water permeability coefficient is shown below [14,38].

$$R_W = \frac{6.84 \times 10^{-8}(18.68 - 0.177x_{BW})}{T_{SW}}. \tag{10}$$

The RO pump net pressure is calculated as shown below [14,38].

$$\Delta P = \frac{\dot{m}_{PW}}{R_W A_m} + \Delta\pi, \tag{11}$$

where A_m is the membrane area.

The power consumption of the *RO* pump can be calculated as shown below [14,38].

$$\dot{W}_{P,RO} = \frac{\Delta P\dot{m}_{SW}}{\rho_{SW}\eta_{P,RO}}, \tag{12}$$

where ρ is the density.

The mass, energy, and concentration balance relationships for the RO system are shown in the Table 3.

Table 3. Mass, energy, and concentration balance relationships for the RO system.

No.	Components	Mass Balance	Energy Equation	x
1	Pump V	$\dot{m}_{22} = \dot{m}_{24}$	$\dot{W}_{PV} = \dot{m}_{22}(h_{24} - h_{22})$	$x_{24} = x_{22}$
2	Pump VI	$\dot{m}_{23} = \dot{m}_{25}$	$\dot{W}_{PIV} = \dot{m}_{23}(h_{25} - h_{23})$	$x_{23} = x_{25}$
3	Membrane I	$\dot{m}_{24} = \dot{m}_{26} + \dot{m}_{27}$	$\dot{m}_{24}h_{24} = \dot{m}_{26}h_{26} + \dot{m}_{27}h_{27}$	$\dot{m}_{24}x_{24} = \dot{m}_{26}x_{26} + \dot{m}_{27}x_{27}$
4	Membrane II	$\dot{m}_{25} = \dot{m}_{28} + \dot{m}_{29}$	$\dot{m}_{25}h_{25} = \dot{m}_{28}h_{28} + \dot{m}_{29}h_{29}$	$\dot{m}_{25}x_{25} = \dot{m}_{28}x_{28} + \dot{m}_{29}x_{29}$
5	Recovery turbine	$\dot{m}_{32} = \dot{m}_{33}$	$\dot{W}_{\text{Recovery turbine}=}\dot{m}_{32}(h_{32} - h_{33})$	$x_{32} = x_{33}$

The following reaction can be considered in the NaClO plant:

$$NaCl + H_2O \rightarrow NaClO + H_2. \quad (13)$$

In the NaClO plant, the following relationships can be considered [14,38]:

$$T_{NaClO} = T_{BW} + 14, \quad (14)$$

$$x_{NaClO} = \frac{1}{6}x_{BW}. \quad (15)$$

The NaClO plant power consumption is as follows [14,38]:

$$\dot{W}_{NaClO} = \frac{10^{-5}(5.9 \times 3600 \times \dot{m}_{NaClO} \times x_{NaClO})}{1.05}. \quad (16)$$

The NaClO plant concentration, mass, and energy balance relationships are shown in Table 4.

Table 4. Mass, energy, and concentration balance relationships for the NaClO plant.

Mass Balance	$\dot{m}_{38} = \dot{m}_{34} + \dot{m}_{35}$
Concentration Balance	$\dot{m}_{38}x_{38} = \dot{m}_{34}x_{34} + \dot{m}_{35}x_{35}$
Energy Balance	$\dot{m}_{38}h_{38} + \dot{W}_{NaClO} = \dot{m}_{34}h_{34} + \dot{m}_{35}h_{35}$

The electrical power production of the system is calculated as follows:

$$\dot{W}_{net,sys} = \sum_{i=1}^{3} \dot{W}_{T,i} + \dot{W}_{recovery\ turbine} - \sum_{i=1}^{6} \dot{W}_{P,i} - \dot{W}_{NaClO}. \quad (17)$$

The system energy efficiency is expressed as

$$\eta_{en,sys} = \frac{\dot{m}_{31}h_{31} + \dot{m}_{34}h_{34} + \dot{m}_{35}h_{35} + \dot{W}_{net,sys} + \dot{Q}_{heater} + \dot{Q}_{cooler}}{\dot{m}_{21}h_{21} + \dot{m}_{10}LHV}. \quad (18)$$

2.1.2. Exergy Analysis

The specific exergy is expressed below, neglecting the kinetic and potential exergies [40,41].

$$e = \sum x_i\, ex_{chi} + (h - h_0) - T_0(s - s_0) + T_0 \sum x_i\, R_i\, lny_i, \quad (19)$$

where x and e are the mass fractions and specific exergy, respectively, T, h, and s are the temperature, specific enthalpy, and specific entropy, respectively, and y denotes the mole fraction. Subscript ch denotes chemical. Abbreviations i and 0 represent the species and the dead state condition.

Table 5 shows the exergy destruction rates and exergy efficiencies for the system components [23,42,43].

Table 5. The exergy destruction rates and exergy efficiencies for system components.

No.	Components	Exergy Efficiency	Exergy Destruction Rate (kW)
		CO_2 cycle	
1	Pump II (P)	$\frac{\dot{W}_{PII}}{\dot{m}_1(e_2-e_1)}$	$\boldsymbol{\dot{m}_1 e_1 - \dot{m}_2 e_2 + \dot{W}_{PII}}$
2	Steam generator	$\frac{\dot{m}_2(e_3-e_2)}{\dot{m}_{17}(e_{17}-e_{18})}$	$\boldsymbol{\dot{m}_2 e_2 + -\dot{m}_3 e_3 + \dot{m}_{17} e_{17} - \dot{m}_{18} e_{18}}$
3	Turbine I (T)	$\frac{\dot{W}_{TI}}{\dot{m}_3(e_3-e_4)}$	$\boldsymbol{\dot{m}_3 e_3 - \dot{m}_4 e_4 - \dot{W}_{TI}}$
4	Condenser	$\frac{\dot{m}_1(e_4-e_1)}{\dot{m}_6(e_7-e_6)}$	$\boldsymbol{\dot{m}_4 e_4 - \dot{m}_1 e_1 + \dot{m}_6 e_6 - \dot{m}_7 e_7}$
		ORC	
5	Pump III (P)	$\frac{\dot{W}_{PIII}}{\dot{m}_1(e_{12}-e_{11})}$	$\boldsymbol{\dot{m}_{11} e_{11} - \dot{m}_{12} e_{12} + \dot{W}_{PIII}}$
6	Evaporator	$\frac{\dot{m}_{12}(e_{13}-e_{12})}{\dot{m}_{17}(e_{36}-e_{37})}$	$\boldsymbol{\dot{m}_{12} e_{12} - \dot{m}_{13} e_{13} + \dot{m}_{36} e_{36} - \dot{m}_{37} e_{37}}$
7	Turbine II (T)	$\frac{\dot{W}_{TII}}{\dot{m}_{13}(e_{13}-e_{14})}$	$\boldsymbol{\dot{m}_{13} e_{13} - \dot{m}_{14} e_{14} - \dot{W}_{TIII}}$
8	Condenser	$\frac{\dot{m}_1(e_{14}-e_{11})}{\dot{m}_6(e_8-e_7)}$	$\boldsymbol{\dot{m}_{14} e_{14} - \dot{m}_{11} e_{11} + \dot{m}_7 e_7 - \dot{m}_8 e_8}$
		LNG loop	
9	Pump I (P)	$\frac{\dot{W}_{PI}}{\dot{m}_5(e_6-e_5)}$	$\boldsymbol{\dot{m}_5 e_5 - \dot{m}_6 e_6 + \dot{W}_{PI}}$
10	Turbine III (T)	$\frac{\dot{W}_{TIII}}{\dot{m}_{13}(e_8-e_9)}$	$\boldsymbol{\dot{m}_8 e_8 - \dot{m}_9 e_9 - \dot{W}_{TIII}}$
11	Cooler	$\frac{\dot{Q}_{cooler}\,(1-\frac{T_9}{T_0})}{\dot{m}_9(e_{10}-e_9)}$	$\boldsymbol{\dot{m}_9 e_9 - \dot{m}_{10} e_{10} - \dot{Q}_{cooler}\,(1-\frac{T_9}{T_0})}$
		Boiler	
12	Boiler	$\frac{\dot{m}_{16}(e_{17}-e_{16})}{\dot{m}_{10} e_{10}}$	$\dot{m}_{16} e_{16} - \dot{m}_{17} e_{17} + \dot{m}_{10} e_{10}$
		Water loop	
13	Pump IV (P)	$\frac{\dot{W}_{PIV}}{\dot{m}_{15}(e_{16}-e_{15})}$	$\boldsymbol{\dot{m}_{15} e_{15} - \dot{m}_{16} e_{16} + \dot{W}_{PIV}}$
14	Heater	$\frac{\dot{Q}_{heater}\,(1-\frac{T_0}{T_{19}})}{\dot{m}_{19}(e_{19}-e_{20})}$	$\boldsymbol{\dot{m}_{19} e_{19} - \dot{m}_{20} e_{20} - \dot{Q}_{heater}\,(1-\frac{T_0}{T_{19}})}$
		RO	
15	Pump V	$\frac{\dot{W}_{PV}}{\dot{m}_{22}(e_{24}-e_{22})}$	$\boldsymbol{\dot{m}_{22}(e_{22}-e_{24}) + \dot{W}_{PV}}$
16	Pump VI	$\frac{\dot{W}_{PVI}}{\dot{m}_{23}(e_{25}-e_{23})}$	$\boldsymbol{\dot{m}_{23}(e_{23}-e_{25}) + \dot{W}_{PVI}}$
17	Membrane I	$\frac{\dot{m}_{26} e_{26}}{\dot{m}_{24} e_{24}}$	$\boldsymbol{\dot{m}_{24} e_{24} - \dot{m}_{27} e_{27} - \dot{m}_{26} e_{26}}$
18	Membrane II	$\frac{\dot{m}_{28} e_{28}}{\dot{m}_{25} e_{25}}$	$\boldsymbol{\dot{m}_{25} e_{25} - \dot{m}_{29} e_{29} - \dot{m}_{28} e_{28}}$
19	Recovery turbine	$\frac{\dot{W}_{recovery\ turbine}}{\dot{m}_{32}(e_{32}-e_{33})}$	$\boldsymbol{\dot{m}_{32} e_{32} - \dot{m}_{33} e_{33} - \dot{W}_{recovery\ turbine}}$
		NaClO	
20	NaClO plant	$\frac{\dot{m}_{34} e_{34} + \dot{m}_{35} e_{35}}{\dot{W}_{NaClO}}$	$\dot{m}_{38} e_{38} + \dot{W}_{NaClO} - \dot{m}_{35} e_{35} - \dot{m}_{34} e_{34}$

The system exergy efficiency is expressed below.

$$\eta_{ex,sys} = \frac{\dot{m}_{31} e_{31} + \dot{m}_{34} e_{34} + \dot{m}_{35} e_{35} + \dot{W}_{net,sys} + \dot{Q}_{heater}\,(1-\frac{T_0}{T_{19}}) + \dot{Q}_{cooler}\,(1-\frac{T_9}{T_0})}{\dot{m}_{21} e_{21} + \dot{m}_5 e_5}. \quad (20)$$

2.1.3. Thermo-Economic Analysis

The multigeneration annual income and outcome are calculated as follows [44,45]:

$$C_F = A_{power}c_{power} + A_{cooling}c_{cooling} + A_{PW}c_{PW} + A_{NaCl}c_{NaCl} + A_{H2}c_{H2} - A_{LNG}c_{LNG}, \quad (21)$$

where c is the specific cost, and A is the annual capacity of system production. The costs of products are shown in Table 6.

Table 6. The specific costs of fuel and products.

Specific Cost	Value	Ref
c_{power}	0.21 USD/kWh	[46]
c_{PW}	0.0004 USD/kg	[47]
$c_{cooling}$/$c_{heating}$	0.07 USD/kWh	[48]
c_{NaCl}	10.47 USD/kg	[49]
c_{H2}	13.96 USD/kg	[50]
c_{LNG}	0.025 USD/kWh	[48]

The system investment cost can be calculated as shown below [44,45].

$$C_0 = C_{ORC} + C_{CO2\ cycle} + C_{LNG\ loop} + C_{Water\ loop} + C_{RO} + C_{NaClO}, \quad (22)$$

where C is the investment cost of each component, as shown in Table 7. The operation and maintenance cost is assumed to be 3% of the initial cost [51-54].

Table 7. Values of investment and installation costs for different components.

No.	Components	Cost Function	Ref
		CO_2 cycle	
1	Pump	$10^{3.3892+0.05361logW+0.1538(logW)^2}$	[23]
2	Steam generator	$(A/0.093)^{0.78}$	[23]
3	Turbine	$10^{2.6259+1.43981logW-0.1776(logW)^2}$	[23]
4	Condenser	$(A/0.093)^{0.78}$	[23]
		ORC	
5	Pump	$1026 \times (\dot{W}/300)^{0.25}$	[55]
6	Evaporator	$216.6 + 353.4 \times A$	[55]
7	Turbine	$2237 \times \dot{W}^{0.41}$	[56]
8	Condenser	$338.6 \times A$	[55]
		LNG loop	
9	LNG turbine	$479.34 \left(\frac{\dot{m}_8}{0.93-\eta_T}\right) \ln\left(\frac{P_8}{P_9}\right)(1-\exp(0.036T_8-54.4))$	[57]
10	LNG pump	$3 \times \exp(8.833 - 0.6019ln(\dot{Q}\sqrt{H}) + 0.06019(\ln(\dot{Q}\sqrt{H}))^2)$	[58]
11	LNG cooler	$1.218 \times \exp(0.4692 + 0.1203\ln(\dot{Q}) + 0.0931(\ln(\dot{Q}))^2)$	[58]
		Water loop	
12	Pump	$3540 \times \dot{W}^{0.71}$	[59]
13	Boiler	33,600,000	[60]
14	Heater	$\eta_{heater}1.218 \times f_d \times f_p \times c_b$ $f_d = \exp(-1.1156 + 0.0906 \times \ln(10.76A))$ $f_p = 0.7771 + 0.04981 \times \ln(10.76A)$ $c_b = \exp(8.821 - 0.30863 \times \ln(10.76A) + 0.0681 \times \ln(10.76A) \times \ln(10.76A))$	[58]
		RO	
15	Pump	$996 \times (864{,}00 \times \dot{Q})^{0.8}$	[61]
16	Membrane	*50*	[62]
17	Storage Tank	$1.14 \times (158{,}62 \times V_{Tank} + 18{,}321)$	[63]
18	Recovery turbine	$52 \times (864{,}00 \times \dot{Q} \times \Delta P^{0.8})$	[61]
		NaClO	
19	NaClO (HD:6000)	45,000	[14]

In Table 7, *A*, *H*, *D*, and *V* denote the surface area, head of pump or turbine, diameter, and volume, respectively.

The logarithmic method is applied to calculate the surface area of the heat exchanger, as shown below [51].

$$\dot{Q} = UAF_t\Delta T_{In}, \tag{23}$$

where $\dot{Q}$ is the heat transfer rate, ΔT_{In} is the logarithmic mean temperature difference, A and U denote the surface area and overall heat transfer coefficient, respectively, and F is the correction factor. The overall heat transfer coefficient values for components are shown in Table 8 [52].

Table 8. The overall heat transfer coefficient values for components.

No.	Components	U (W/m^2K)
2	Boiler	500
3	Heat exchanger	700
4	Condenser	800

The effect of inflation can be seen in the following relationship [64]:

$$C_n = C_0(1+i)^n, \tag{24}$$

where *i* and *n* are the inflation rate (3%) and the number of years, respectively [65].

The simple payback period (SPP) can be calculated as shown below [44,45].

$$SPP = \frac{C_n}{CF}. \tag{25}$$

The payback period (*PP*) can be calculated as shown below [66,44,45].

$$PP = \frac{ln(\frac{C_F}{CF - r.C_n})}{ln(1+r)}, \tag{26}$$

where *r* is the discount factor (3%).

The net present value (NPV) can be obtained as follows [44,45]:

$$NPV = CF\frac{(1+r)^N - 1}{r(1+r)^N} - C_n, \tag{27}$$

where *N* is the project lifetime (25 years) [44,45].

The internal rate of return (IRR) can be calculated as follows [67,68,55]:

$$IRR = \frac{CF}{C_n}\left[1 - \frac{1}{(1+IRR)^N}\right]. \tag{28}$$

3. Results and Discussion

3.1. Simulation Method Description

For the simulation, a computer code provided in the engineering equation solver (EES) software was used. The computer code input information is shown in Table 9.

Table 9. Input information of the simulation code.

Parameter	Unit	Value	Ref
$\dot{m}_1$	kg/s	6.73	[41]
T_1	K	220	[41]
T_2	K	224.9	[41]
T_3	K	493.1	[41]
P_1	kPa	600	[41]
P_2	kPa	12,490	[41]

x_{21}	mg/L	40,200	[69]
x_{30}	mg/L	150	[69]
A_m	m²	35.3	[70]
RR	-	0.3	[14]
$\dot{m}_{21}$	kg/s	2	-

3.2. Model Validation

Since the proposed plant had a new configuration, its complete validation was not achievable. Hence, each subsystem was considered. To validate the CO_2 cycle and LNG loop, the results in [32] were considered. Four key parameters (CO_2 and LNG turbine power production and pump power production) were compared. Table 10 shows a comparison between the present work and the results in [32]. The source of error was related to the calculation of thermodynamic properties, which features slight differences in each software.

To validate the ORC results, Figure 2 in [56] was considered. R600a was selected as the working fluid. The data for the ORC presented in [56] were used. Figure 3 shows a comparison between the net output power of this work and the results in [56]. The maximum error was 3.5%, which is compatible with engineering calculations. The source of error was similar to that of the CO_2 cycle.

Table 10. The comparison of key parameters in the present work and in [32].

No.	Parameter	Unit	Present Work	Ref [32]	Error (%)
1	$\dot{W}_{T,CO2}$	kW	14.2	14.66	3.1
2	$\dot{W}_{P,CO2}$	kW	4.98	4.778	4.2
3	$\dot{W}_{T,LNG}$	kW	7.19	7.464	3.6
4	$\dot{W}_{P,LNG}$	kW	3.81	3.693	3.1

For RO validation, the results in [14] were used. Table 11 shows the comparison. The error ranged from 0.7% to 7% due to some information about membrane performance not being exactly clarified in [14] For NaClO plant validation, the results in [57] were used. The electrical power consumption of the NaClO plant was found to be 4 kW, while this value was theoretically calculated as 3.78 kW by the computer code. The error of 5.5% was related to the type and model of the NaClO plant.

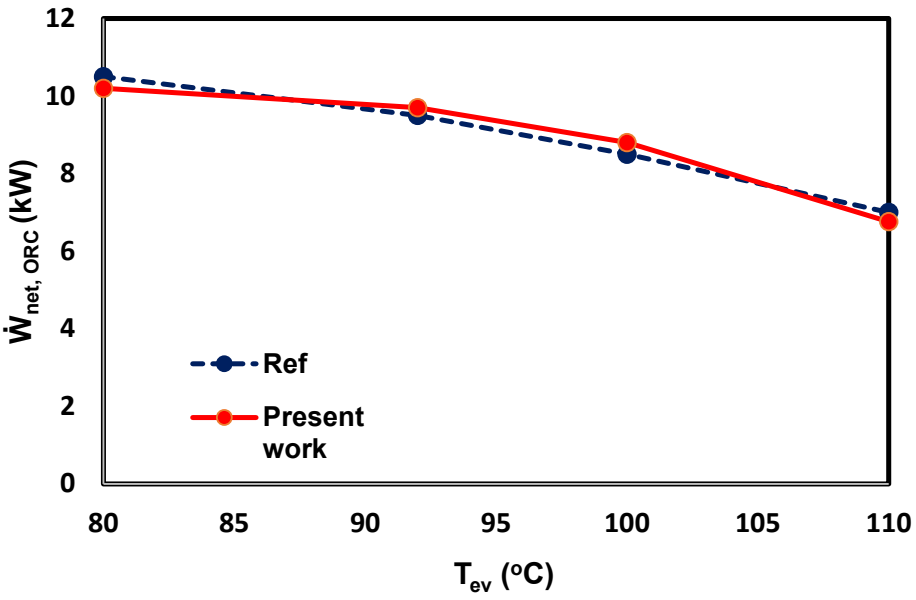

Figure 3. Comparison of the net output power in the present work with that in [14] versus the evaporator temperature of the ORC.

Table 11. Validation results of the RO system.

No.	Parameter	Model	Ref [14]	Error (%)
10	$\dot{m}_{brain}(\frac{kg}{s})$	1.092	1.104	0.7
2	$\dot{m}_{brain}(\frac{kg}{s})$	0.468	0.456	2.6
3	$\dot{m}_{brain}(\frac{kg}{s})$	3.45	3.711	7
4	$\dot{m}_{brain}(\frac{kg}{s})$	8.42	8.96	6

3.3. Energy and Exergy Analyses

Table 12 shows the thermodynamic properties at every point of the system. Table 13 shows the values of the system products. This system produces 10.53 GWh of electrical energy, 276.4 GWh of cooling energy, 1783 GWh of heating energy, 17,280 m^3 of potable water, 739.56 tons of hydrogen, and 383.78 tons of salt in a year. The ratios of cooling and heating energies to electrical energy are 26.25 and 169.33, respectively. Figure 4 shows the system energy and exergy efficiencies. According to the figure, the energy and exergy efficiencies are 54.3% and 13.1%, respectively. The system energy efficiency is much higher than the system exergy efficiency, as, in the exergy efficiency equation (Equation (20)), both the heat and the cooling production rates are multiplied by the ratios, which are lower than the unit. The variation in RO and NaClO plant power consumption and in recovery turbine and system power productions versus seawater inlet mass flow rate ($\dot{m}_{21}$) is shown in Figure 5. Upon increasing the $\dot{m}_{21}$ from 1 to 5 kg/s, the power consumption of the RO and NaClO plant can be increased from 1.486 and 134.8 kW to 35.7 and 673.9 kW, respectively. According to the equations presented in Table 3, the power consumption of the RO pumps has a linear relationship with the mass flow rate of feed water. According to Equation (16), the power consumption of the NaClO plant also has a linear relationship with feed brain water.

The net electrical power production of the total proposed system is reduced from 1456.7 kW to 876.7 kW following this increase in $\dot{m}_{21}$.

Table 12. The thermodynamic properties at every point of the system.

No	T (K)	P (kPa)	$\dot{m}$ (kg/s)	X (-)	h (kJ/kg)	e (kJ/kg)
1	220.0	600	6.73	-	−420	210.7
2	224.9	12,490	6.73	-	−407.2	220.1
3	493.2	12,490	6.73	-	141	288.3
4	220.5	610	6.73	-	−74.91	104.7
5	111.5	101.4	9.547	-	−911.7	1015
6	115.3	6580	9.547	-	−889	1019
7	210.5	6440	9.547	-	−372.5	655.8
8	283.2	6310	9.547	-	−104.5	599.4
9	255.3	4000	9.547	-	−148.7	542.9
10	288.2	4000	9.547	-	−4672	548.9
11	271.9	280	10.26	-	50.18	35.22
12	295.3	709.1	10.26	-	89.45	35.27
13	403.2	709.1	10.26	-	369.2	60.63
14	272.9	280	10.26	-	249.7	23.31
15	303.2	101.3	115.5	-	125.8	1.579
16	303.2	150	115.5	-	125.8	1.627

17	513.2	150	115.5	-	2952	705
18	493.2	150	115.5	-	2912	687.9
19	493.2	150	114.3	-	2912	687.9
20	303.2	101.3	114.3	-	125.8	1.579
21	288.2	101.3	2	40,020	59.45	13.46
22	288.2	101.3	1	40,020	59.45	13.46
23	288.2	101.3	1	40,020	59.45	13.46
24	288.2	4767	1	40,020	63.69	17.98
25	288.2	4767	1	40,020	63.69	17.98
26	288.2	4767	0.3	150	67.49	4.659
27	288.2	4767	0.7	57,107	61.83	6.596
28	288.2	4767	0.3	150	67.49	4.659
29	288.2	4767	0.7	57,107	61.83	6.596
30	288.2	4767	0.6	150	67.49	4.659
31	288.2	101.3	0.6	150	63.05	0.000242
32	288.2	4767	1.4	57,107	61.83	6.596
33	288.2	303.9	1.4	57,107	57.84	2.323
34	507.2	101.3	0.01333	-	205.9	156.5
35	298.2	101.3	0.02568	-	7885	1226
36	493.2	150	1.288	-	2912	687.9
37	303.2	101.3	1.288	-	125.8	1.579
38	288.2	101.3	14	-	57.84	2.323

Table 13. The values of system products.

Product	Unit	Value
$\mathbf{W_{net,system}}$	GWh/year	12.75
$\mathbf{Q_{cooling}}$	GWh/year	276.4
$\mathbf{Q_{heating}}$	GWh/year	1783
$\mathbf{V_{PW}}$	m^3/year	17280
$\mathbf{m_{NaCl}}$	Ton/year	383.76
$\mathbf{m_{H2}}$	Ton/year	739.56

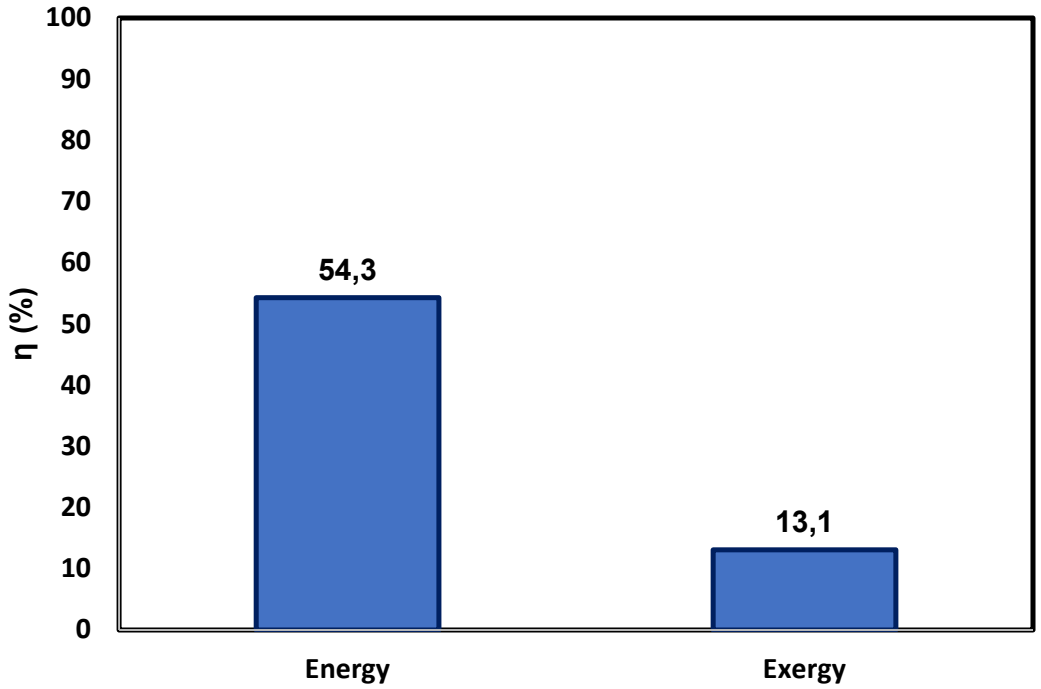

Figure 4. The system energy and exergy efficiencies.

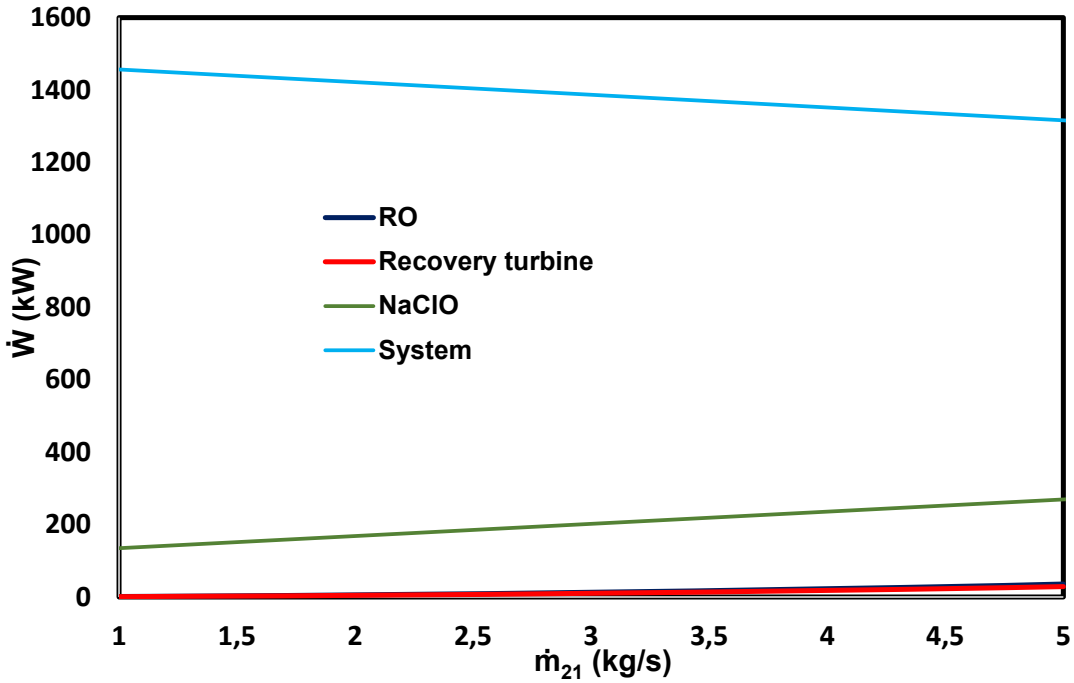

Figure 5. The variation in RO, NaClO plant, recovery turbine, and system power with inlet seawater mass flow rate ($\dot{m}_{21}$).

The system energy and exergy efficiencies versus seawater mass flow rate ($\dot{m}_{21}$) are shown in Figure 6. Increasing the seawater mass flow rate did not have a major effect on the system energy and exergy efficiencies. Upon increasing the seawater mass flow rate from 1 to 5 kg/s, the system energy and exergy efficiencies were reduced from 54.25% and

13.11% to 54.23% and 13.01%, respectively. It can be concluded that the system energy and exergy efficiencies remained constant. Since the extra electrical power consumed by the NaClO and RO systems is compensated for by the extra energy and exergy flows of PW, NaCl, and hydrogen, according to Equations (18) and (20).

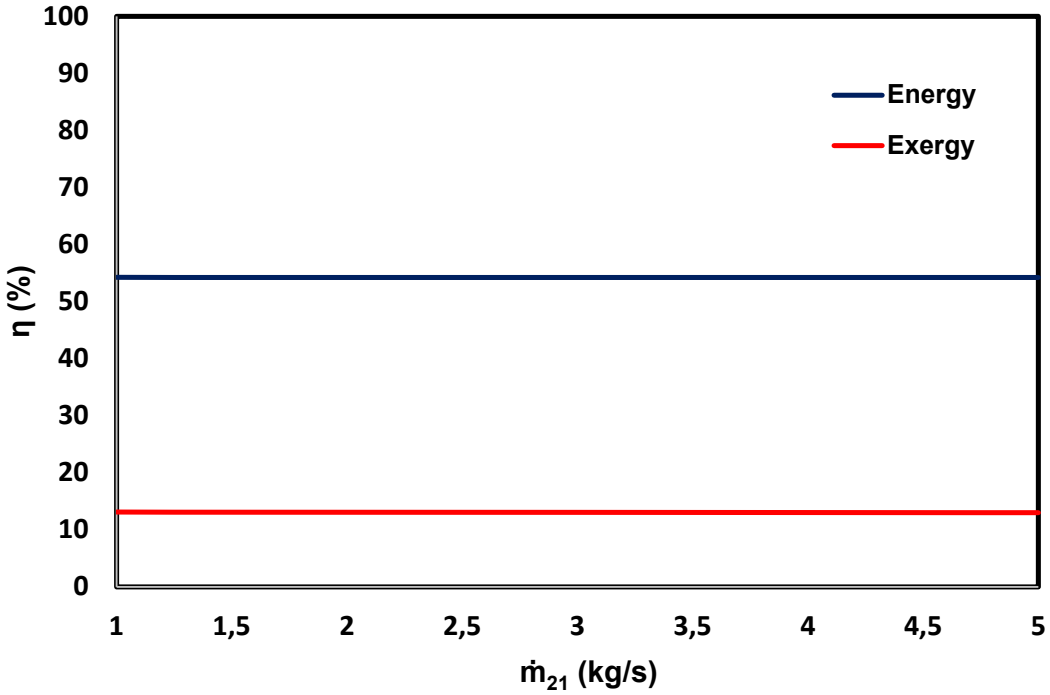

Figure 6. The system energy and exergy efficiencies versus seawater mass flow rate ($\dot{m}_{21}$).

Figure 7 shows the changes in pump electrical power consumption and turbine electrical power production, as well as the net output power of the CO_2 cycle, with the variation in outlet pressure of the pump (P_2) in the CO_2 cycle. Upon increasing the outlet pressure of the pump, the electrical power consumption of the pump in the CO_2 cycle is increased. Moreover, the electrical power production of the turbine is decreased. This is because the superheat temperature at point 3 is fixed at 493.1 K (above the supercritical temperature), which is about 293.1 K less than the superheated steam temperature at point 17 according to pinch analysis.

Thus, by increasing the outlet pressure of the pump in the CO_2 cycle (P_2) at a fixed temperature (493.1 K), the enthalpy at point 3 is reduced, and the electrical power production in the turbine is reduced. It is clear that, by increasing the electrical power consumption of the pump and the electrical power production of the turbine, the net electrical power of the CO_2 cycle is decreased.

Figure 8 shows the variation in CO_2 cycle energy and exergy efficiencies with outlet pump pressure in the CO_2 cycle. According to Figure 7, the CO_2 cycle net output electrical power is reduced upon increasing the outlet pressure of the pump, whereas the inlet heat rate of the CO_2 cycle ($\dot{m}$ (h_{17}–h_{18})) remains constant.

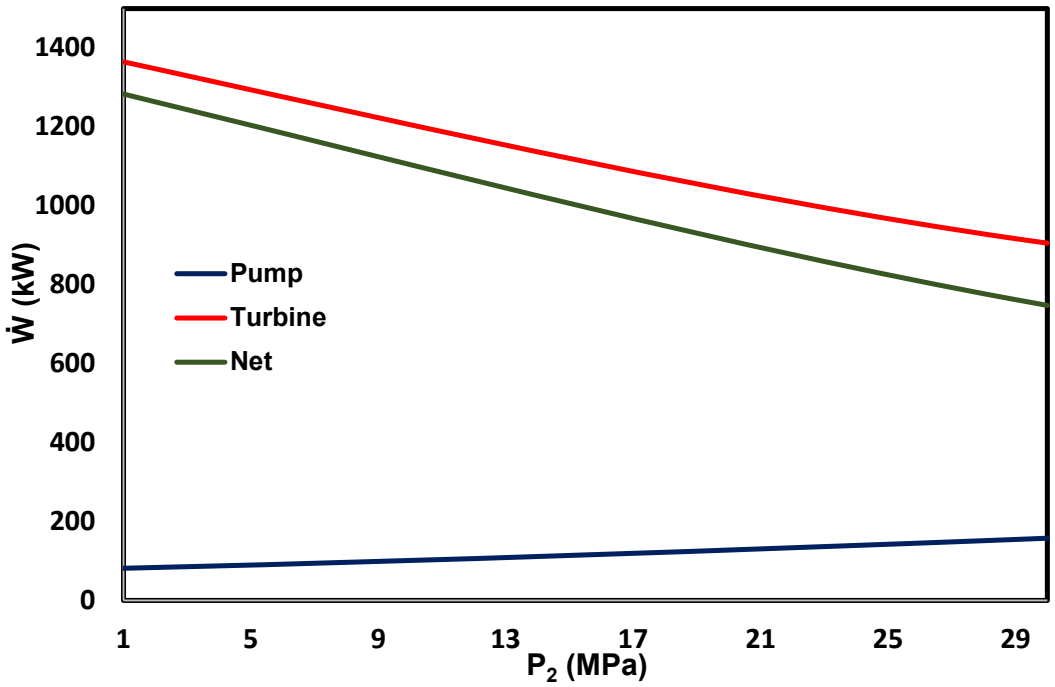

Figure 7. The changes in pump and turbine electrical power consumption/production and net output power of the CO_2 cycle with the variation in pump outlet pressure (P_2) in the CO_2 cycle.

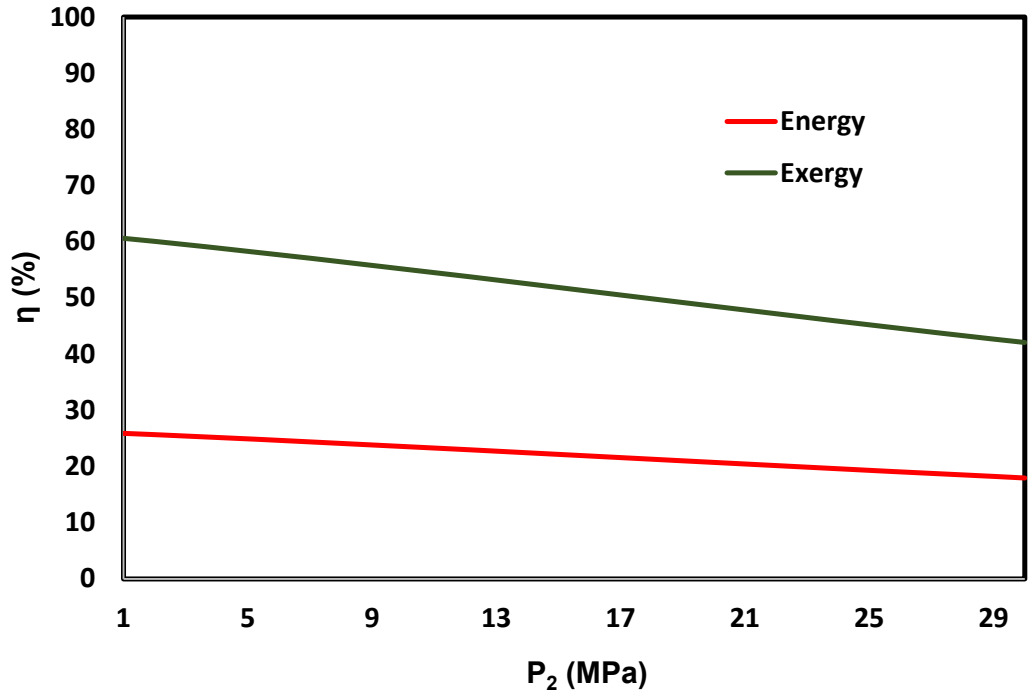

Figure 8. The variation in CO_2 cycle energy and exergy efficiencies with outlet pump pressure in the CO_2 cycle.

The change in net output power of the ORC with pump outlet pressure at different inlet turbine temperatures is shown in Figure 9. Upon increasing the ORC pump outlet pressure, the cycle net output power is reduced, since it decreases the enthalpy value at

point 13. Furthermore, the power consumption of the pump increases. Upon increasing the turbine inlet temperature in the ORC, the net output electrical power is increased by increasing the enthalpy at point 13.

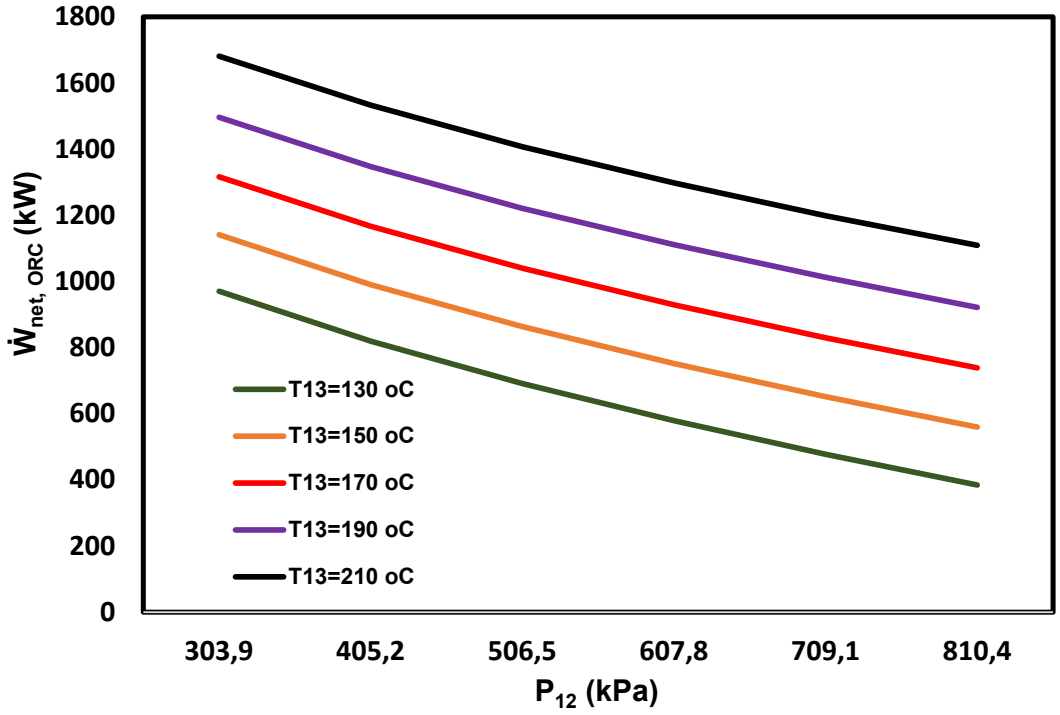

Figure 9. The variation in net output power of the ORC with pump outlet pressure at different inlet turbine temperatures.

The contribution to exergy destruction rate of each subsystem is presented in Figure 10. The highest contribution comes from the water loop, which includes a heater, burner/boiler, and pump IV. In the burner, a chemical reaction (combustion) warms the water in the boiler, thereby converting water to steam. Thus, this loop has the highest exergy destruction rate. In distant second place, the CO_2 cycle has a considerable exergy destruction rate due to the heat transfer taking place in the steam generator and condenser. The lowest exergy destruction rate occurs in the RO system, as the pressures and temperatures in this system are all close to the dead state.

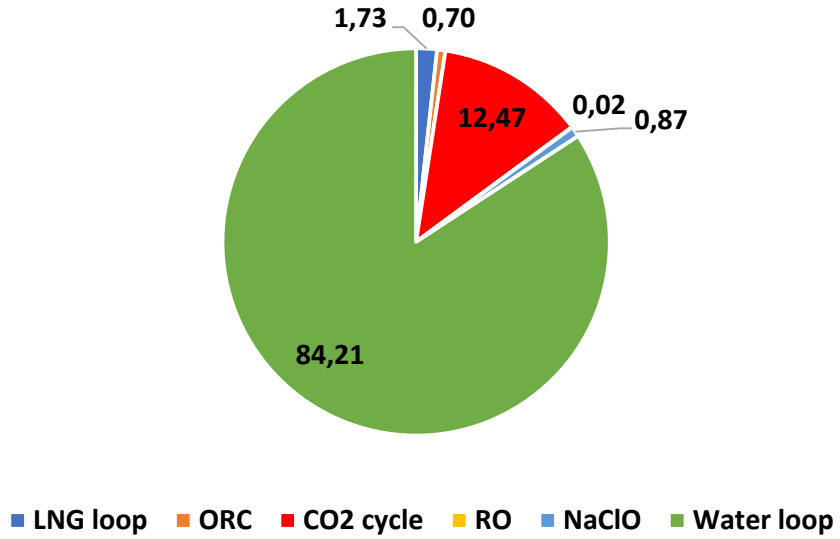

Figure 10. Contributions of each system to the exergy destruction rate.

3.4. Thermo-Economic Analyses

Table 14 shows the key economic parameters for the system. The system's NPV is 908.9 million USD, the system's PP and SPP are equal to 7.9 and 6.9 years, and the system's IRR is 0.138.

Table 14. The key economic parameters for the system.

No.	Parameter	Unit	Value
1	NPV	million USD	908.9
2	PP	years	7.9
3	SPP	years	6.9
4	IRR	-	0.138

Figure 11 shows the variation in PP and SPP versus feed seawater mass flow rate. Upon increasing the seawater mass flow rate, both PP and SPP are reduced, which is beneficial. Specifically, upon increasing the feed seawater mass flow rate from 1 kg/s to 5 kg/s, the PP is reduced from 8.7 to 6.2 years and the SPP is reduced from 7.56 to 5.59 years.

In general, increasing the seawater mass flow causes the following effects:

(a) Increase in the initial cost of the NaClO and RO plants (negative effect);
(b) Increase in the system product costs (NaCl, PW, and hydrogen) due to an increase in these products;
(c) Decrease in the electrical power product cost due to an increase in RO and NaClO plant power consumption.

The magnitude of the second effect exceeds that of the other two effects; thus, both PP and SPP are reduced upon increasing the feed seawater mass flow rate.

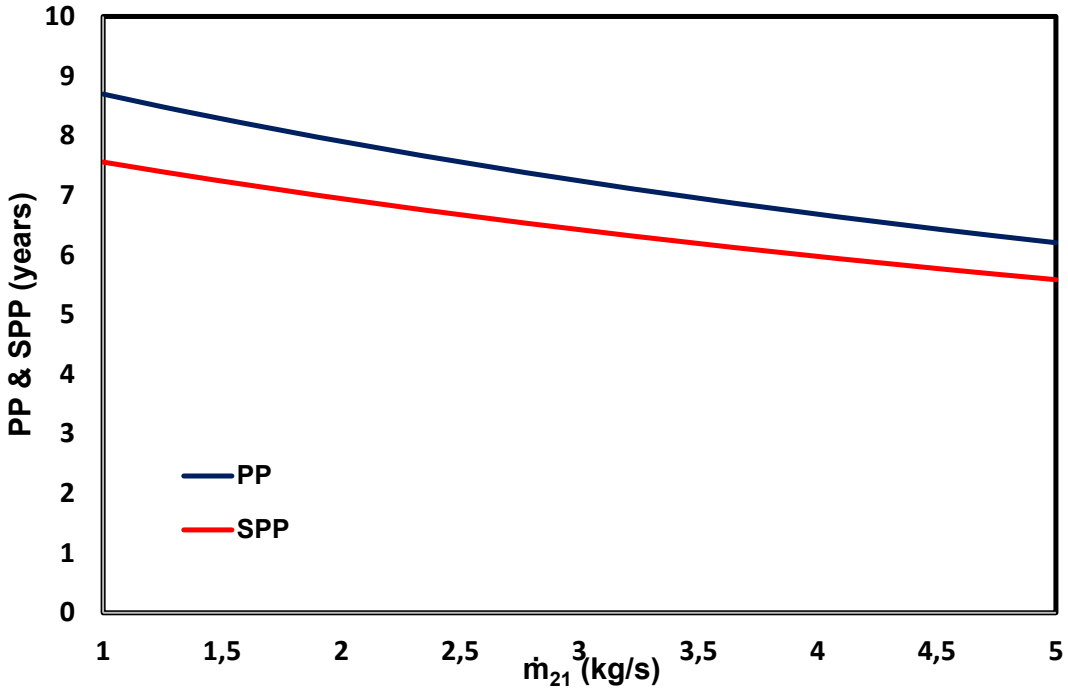

Figure 11. The variation in PP and SPP versus feed seawater mass flow rate.

The variation in system NPV with the mass flow rate of seawater is depicted in Figure 12. The NPV of the system is increased upon increasing the mass flow rate of seawater. Similar to Figure 11, it is clear that, if more electrical power is consumed to produce PW, NaCl, and hydrogen, it is more beneficial.

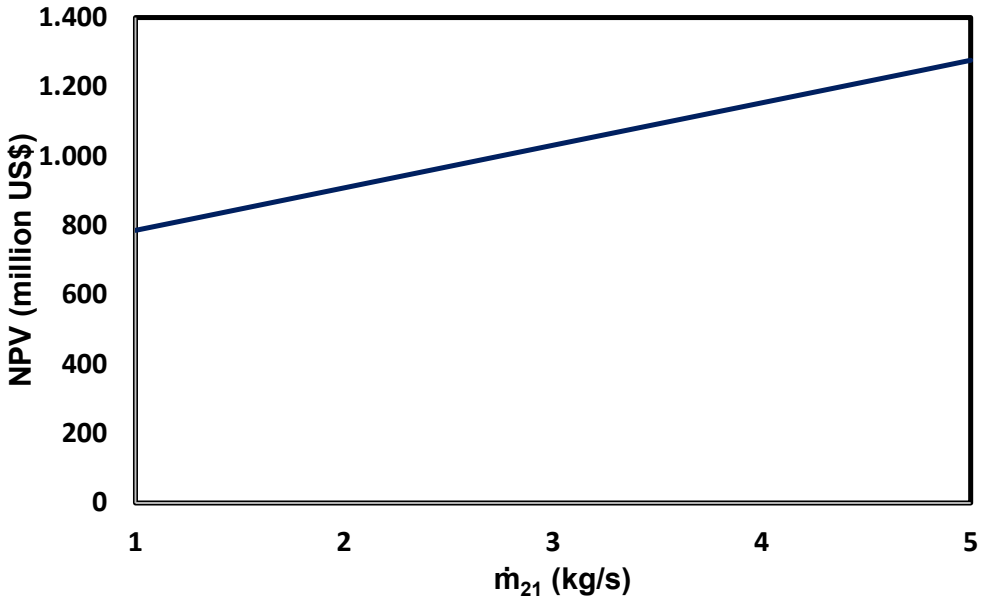

Figure 12. The variation in system NPV with the feed seawater mass flow rate.

4. Conclusions

A new integrated system was proposed in this paper which simultaneously uses LNG as a heat source and sink. Through this method, the ratio of the heat sink and source temperatures is high, thereby improving system performance.

The CO_2 cycle and ORC are combined to generate electricity in this proposed system. In both cycles, LNG is used to absorb the heat dissipated by condensers, as well as to produce cooling load. Subsequently, the LNG is converted to NG. The NG is used to convert water into steam in the burner and boiler, thus meeting the energy needs of the steam generator and evaporator in the CO_2 cycle and the ORC, in addition to producing heating load. A portion of the electrical power generated in the two mentioned cycles is used to produce hydrogen, salt, and PW in the RO and NaClO plants. The main conclusions are summarized below.

(a) In comparison with a system featuring LNG only as a heat sink [14], which uses solar energy through a flat plate collector as the heat source, the system energy and exergy efficiencies are further improved from 12.4% and 4.45% to 54% and 13.1%, respectively.
(b) The NPV of this system is equal to 908.9 million USD.
(c) The PP and SPP of this system are 7.9 and 6.9 years, respectively.
(d) The IRR value of this system is equal to 0.138.
(e) Greater desalination of seawater to produce PW, salt, and hydrogen is beneficial according to the economic evaluation.
(f) Greater seawater desalination does not have a considerable effect on the system energy and exergy efficiencies.
(g) The highest and lowest contributions to the exergy destruction rates were presented by the water loop and RO system.

In the future, the integration of various cycles such as the Kalina and Goswami cycles can be examined as alternatives.

Author Contributions: Conceptualization, T.T., M.A.E., and A.A.; methodology, T.T. and M.A.E.; software, T.T. and M.A.E.; validation, M.A.E., A.A., and S.H.; formal analysis, T.T., M.A.E., and A.A.; investigation, M.A.E. and A.A.; resources, T.T. and M.A.E.; data curation, M.A.E.; writing—original draft preparation, M.A.E., A.A., and S.H.; writing—review and editing, S.M., S.H., M.A.E., and A.A.; visualization, T.T., M.A.E., S.M., S.H., and A.A.; project administration, T.T., M.A.E., A.A., S.H., and S.M.; funding acquisition, M.A.E., A.A., S.H., and S.M. All authors have read and agreed to the published version of the manuscript.

Funding: This research received no external funding.

Institutional Review Board Statement: Not Applicable.

Informed Consent Statement: Not Applicable.

Data Availability Statement: Not applicable.

Acknowledgments: The authors would like to express their appreciation for the financial and scientific assistance provided by Hasan Barzegar and Ali Rajaei from the Energy Optimization Research and Development Group (EORD), Tehran, Iran.

Conflicts of Interest: The authors declare no conflicts of interest.

Nomenclature

Symbols (units)	*Description*
A (m^2)	Area
$\mathbf{C_0}$ (USD)	System investment cost
$\mathbf{C_n}$ (USD)	System investment cost in a specific year
CF (USD)	Multigeneration annual income
e (kJ/kg)	Specific exergy
$\dot{E}$ (kW)	Exergy rate

F_t (-)	Correction factor
g (m/s^2)	Gravitational acceleration
h (kJ/kg)	Specific enthalpy
c (USD/kWh)	Product-specific cost
C (USD)	Investment cost
R_W (1/K)	Water permeability coefficient
$\dot{m}$ (kg/s)	Mass flow rate
N (years)	Project lifetime
P (kPa)	Pressure
$\dot{Q}$ (kW)	Heat transfer rate
r (-)	Discount factor
R (kJ/kmoleK)	Global gas constant
s (kJ/kgK)	Specific entropy
T	Temperature
U (W/m^2K)	Overall heat transfer coefficient
V (m^3)	Volume
$\dot{W}$ (kW)	Power
***x* (-)**	Mass fraction, concentration of salt
y (-)	Mole fraction
Y (USD/kWh, USD/kg)	Annual capacity of system production

Greek Symbols	*Description*
η(-)	Polythrophic efficiency
$\Delta\pi$ (Pa)	Net pressure membrane

Abbreviations	*Description (Units)*
IRR	Internal rate of return (-)
NPV	Net present value (USD)
PP	Payback period (-)
RR	Recovery ratio (years)
SPP	Simple payback period (kW)
	Exergy rate (kW)

References

1. Omoregie, U. After the Crash: Oil Price Recovery and LNG Project Viability. *Nat. Resour.* **2019**, *10*, 179–186, doi:10.4236/nr.2019.105012.
2. Ehyaei, M.; Ahmadi, A.; Assad, M.E.H.; Rosen, M.A. Investigation of an integrated system combining an Organic Rankine Cycle and absorption chiller driven by geothermal energy: Energy, exergy, and economic analyses and optimization. *J. Clean. Prod.* **2020**, *258*, 120780, doi:10.1016/j.jclepro.2020.120780.
3. Kumar, S.; Kwon, H.-T.; Choi, K.-H.; Lim, W.; Cho, J.H.; Tak, K.; Moon, I. LNG: An eco-friendly cryogenic fuel for sustainable development. *Appl. Energy* **2011**, *88*, 4264–4273, doi:10.1016/j.apenergy.2011.06.035.
4. Chen, Y.; He, L.; Guan, Y.; Lu, H.; Li, J. Life cycle assessment of greenhouse gas emissions and water-energy optimization for shale gas supply chain planning based on multi-level approach: Case study in Barnett, Marcellus, Fayetteville, and Haynesville shales. *Energy Convers. Manag.* **2017**, *134*, 382–398, doi:10.1016/j.enconman.2016.12.019.
5. Lv, Q.; Liu, H.; Wang, J.; Liu, H.; Shang, Y. Multiscale analysis on spatiotemporal dynamics of energy consumption CO2 emissions in China: Utilizing the integrated of DMSP-OLS and NPP-VIIRS nighttime light datasets. *Sci. Total. Environ.* **2020**, *703*, 134394, doi:10.1016/j.scitotenv.2019.134394.
6. Uwitonze, H.; Han, S.; Jangryeok, C.; Hwang, K.S. Design process of LNG heavy hydrocarbons fractionation: Low LNG temperature recovery. *Chem. Eng. Process. Process. Intensif.* **2014**, *85*, 187–195, doi:10.1016/j.cep.2014.09.002.
7. Nakaiwa, M.; Akiya, T.; Owa, M.; Tanaka, Y. Evaluation of an energy supply system with air separation. *Energy Convers. Manag.* **1996**, *37*, 295–301, doi:10.1016/0196-8904(95)00787-3.

8. Messineo, A.; Panno, G. LNG cold energy use in agro-food industry: A case study in Sicily. *J. Nat. Gas Sci. Eng.* **2011**, *3*, 356–363, doi:10.1016/j.jngse.2011.02.002.
9. Wang, P.; Chung, T.-S. A conceptual demonstration of freeze desalination–membrane distillation (FD–MD) hybrid desalination process utilizing liquefied natural gas (LNG) cold energy. *Water Res.* **2012**, *46*, 4037–4052, doi:10.1016/j.watres.2012.04.042.
10. Jansen, S.; Woudstra, N. Understanding the exergy of cold: theory and practical examples. *Int. J. Exergy* **2010**, *7*, 693–713, doi:10.1504/ijex.2010.035516.
11. Liu, E.; Lv, L.; Yi, Y.; Xie, P. Research on the Steady Operation Optimization Model of Natural Gas Pipeline Considering the Combined Operation of Air Coolers and Compressors. *IEEE Access* **2019**, *7*, 83251–83265, doi:10.1109/access.2019.2924515.
12. Otsuka, T. Evolution of an LNG terminal: Senboku Terminal of Osaka gas. In Proceedings of the 23rd World Gas Conference, Amsterdam, The Netherlands, 5–9 June 2006; pp. 2617–2630.
13. Li, Z.-G.; Cheng, H.; Gu, T.-Y. Research on dynamic relationship between natural gas consumption and economic growth in China. *Struct. Chang. Econ. Dyn.* **2019**, *49*, 334–339, doi:10.1016/j.strueco.2018.11.006.
14. Naseri, A.; Bidi, M.; Ahmadi, M.H. Thermodynamic and exergy analysis of a hydrogen and permeate water production process by a solar-driven transcritical CO_2 power cycle with liquefied natural gas heat sink. *Renew. Energy* **2017**, *113*, 1215–1228, doi:10.1016/j.renene.2017.06.082.
15. Qi, M.; Park, J.; Kim, J.; Lee, I.; Moon, I. Advanced integration of LNG regasification power plant with liquid air energy storage: Enhancements in flexibility, safety, and power generation. *Appl. Energy* **2020**, *269*, 115049, doi:10.1016/j.apenergy.2020.115049.
16. Franco, A.; Casarosa, C. Thermodynamic analysis of direct expansion configurations for electricity production by LNG cold energy recovery. *Appl. Therm. Eng.* **2015**, *78*, 649–657, doi:10.1016/j.applthermaleng.2014.11.062.
17. Yu, H.; Kim, D.; Gundersen, T. A study of working fluids for Organic Rankine Cycles (ORCs) operating across and below ambient temperature to utilize Liquefied Natural Gas (LNG) cold energy. *Energy* **2019**, *167*, 730–739, doi:10.1016/j.energy.2018.11.021.
18. Ahmadi, A.; El Haj Assad, M.; Jamali, D.; Kumar, R.; Li, Z.; Salameh, T.; Al-Shabi, M.; Ehyaei, M. Applications of geothermal organic Rankine Cycle for electricity production. *J. Clean. Prod.* **2020**, *274*, 122950, doi:10.1016/j.jclepro.2020.122950.
19. Ghaebi, H.; Namin, A.S.; Rostamzadeh, H. Exergoeconomic optimization of a novel cascade Kalina/Kalina cycle using geothermal heat source and LNG cold energy recovery. *J. Clean. Prod.* **2018**, *189*, 279–296, doi:10.1016/j.jclepro.2018.04.049.
20. Angelino, G.; Invernizzi, C.M. The role of real gas Brayton cycles for the use of liquid natural gas physical exergy. *Appl. Therm. Eng.* **2011**, *31*, 827–833, doi:10.1016/j.applthermaleng.2010.10.032.
21. Ahmadi, A.; Jamali, D.; Ehyaei, M.; Assad, M.E.H. Energy, exergy, economic and exergoenvironmental analyses of gas and air bottoming cycles for production of electricity and hydrogen with gas reformer. *J. Clean. Prod.* **2020**, *259*, 120915, doi:10.1016/j.jclepro.2020.120915.
22. Pattanayak, L.; Padhi, B.N. Thermodynamic analysis of combined cycle power plant using regasification cold energy from LNG terminal. *Energy* **2018**, *164*, 1–9, doi:10.1016/j.energy.2018.08.187.
23. Ahmadi, M.H.; Mehrpooya, M.; Pourfayaz, F. Exergoeconomic analysis and multi objective optimization of performance of a Carbon dioxide power cycle driven by geothermal energy with liquefied natural gas as its heat sink. *Energy Convers. Manag.* **2016**, *119*, 422–434, doi:10.1016/j.enconman.2016.04.062.
24. Xue, X.; Guo, C.; Du, X.; Yang, L.; Yang, Y. Thermodynamic analysis and optimization of a two-stage organic Rankine cycle for liquefied natural gas cryogenic exergy recovery. *Energy* **2015**, *83*, 778–787, doi:10.1016/j.energy.2015.02.088.
25. Xu, J.; Lin, W. A CO2 cryogenic capture system for flue gas of an LNG-fired power plant. *Int. J. Hydrog. Energy* **2017**, *42*, 18674–18680, doi:10.1016/j.ijhydene.2017.04.135.
26. Stradioto, D.A.; Seelig, M.F.; Schneider, P.S. Reprint of: Performance analysis of a CCGT power plant integrated to a LNG regasification process. *J. Nat. Gas Sci. Eng.* **2015**, *27*, 18–22, doi:10.1016/j.jngse.2015.06.009.
27. Shi, X.; Agnew, B.; Che, D.; Gao, J. Performance enhancement of conventional combined cycle power plant by inlet air cooling, inter-cooling and LNG cold energy utilization. *Appl. Therm. Eng.* **2010**, *30*, 2003–2010, doi:10.1016/j.applthermaleng.2010.05.005.
28. Atienza-Márquez, A.; Bruno, J.C.; Akisawa, A.; Coronas, A. Performance analysis of a combined cold and power (CCP) system with exergy recovery from LNG-regasification. *Energy* **2019**, *183*, 448–461, doi:10.1016/j.energy.2019.06.153.
29. Ayou, D.S.; Eveloy, V. Energy, exergy and exergoeconomic analysis of an ultra low-grade heat-driven ammonia-water combined absorption power-cooling cycle for district space cooling, sub-zero refrigeration, power and LNG regasification. *Energy Convers. Manag.* **2020**, *213*, 112790, doi:10.1016/j.enconman.2020.112790.
30. Taheri, M.; Mosaffa, A.; Farshi, L.G. Energy, exergy and economic assessments of a novel integrated biomass based multigeneration energy system with hydrogen production and LNG regasification cycle. *Energy* **2017**, *125*, 162–177, doi:10.1016/j.energy.2017.02.124.
31. Liu, Y.; Han, J.; You, H. Performance analysis of a CCHP system based on SOFC/GT/CO2 cycle and ORC with LNG cold energy utilization. *Int. J. Hydrog. Energy* **2019**, *44*, 29700–29710, doi:10.1016/j.ijhydene.2019.02.201.
32. Naseri, A.; Bidi, M.; Ahmadi, M.H.; Saidur, R. Exergy analysis of a hydrogen and water production process by a solar-driven transcritical CO 2 power cycle with Stirling engine. *J. Clean. Prod.* **2017**, *158*, 165–181, doi:10.1016/j.jclepro.2017.05.005.
33. Ferrero García, R.; Carbia Carril, J.; Romero Gomez, J.; Romero Gomez, M. Power plant based on three series Rankine cycles combined with a direct expander using LNG cold as heat sink. *Energy Convers. Manag.* **2015**, *101*, 285–294, doi:10.1016/j.enconman.2015.05.051.

34. Pan, Z.; Zhang, L.; Zhang, Z.; Shang, L.; Chen, S. Thermodynamic analysis of KCS/ORC integrated power generation system with LNG cold energy exploitation and CO2 capture. *J. Nat. Gas Sci. Eng.* **2017**, *46*, 188–198, doi:10.1016/j.jngse.2017.07.018.
35. Xia, W.; Huo, Y.; Song, Y.; Han, J.; Dai, Y. Off-design analysis of a CO2 Rankine cycle for the recovery of LNG cold energy with ambient air as heat source. *Energy Convers. Manag.* **2019**, *183*, 116–125, doi:10.1016/j.enconman.2018.12.098.
36. Behzadi, A.; Gholamian, E.; Ahmadi, P.; Habibollahzade, A.; Ashjaee, M. Energy, exergy and exergoeconomic (3E) analyses and multi-objective optimization of a solar and geothermal based integrated energy system. *Appl. Therm. Eng.* **2018**, *143*, 1011–1022, doi:10.1016/j.applthermaleng.2018.08.034.
37. Ghasemian, E.; Ehyaei, M.A. Evaluation and optimization of organic Rankine cycle (ORC) with algorithms NSGA-II, MOPSO, and MOEA for eight coolant fluids. *Int. J. Energy Environ. Eng.* **2017**, *9*, 39–57, doi:10.1007/s40095-017-0251-7.
38. Bejan, A. *Advanced Engineering Thermodynamics*; John Wiley & Sons: Hoboken, NJ, USA, 2016.
39. Li, Z.; Ehyaei, M.; Kamran Kasmaei, H.; Ahmadi, A.; Costa, V. Thermodynamic modeling of a novel solar powered quad generation system to meet electrical and thermal loads of residential building and syngas production. *Energy Convers. Manag.* **2019**, *199*, 111982, doi:10.1016/j.enconman.2019.111982.
40. Talebizadehsardari, P.; Ehyaei, M.; Ahmadi, A.; Jamali, D.; Shirmohammadi, R.; Eyvazian, A.; Ghasemi, A.; Rosen, M.A. Energy, exergy, economic, exergoeconomic, and exergoenvironmental (5E) analyses of a triple cycle with carbon capture. *J. CO2 Util.* **2020**, *41*, 101258, doi:10.1016/j.jcou.2020.101258.
41. Yargholi, R.; Kariman, H.; Hoseinzadeh, S.; Bidi, M.; Naseri, A. Modeling and advanced exergy analysis of integrated reverse osmosis desalination with geothermal energy. *Water Sci. Technol. Water Supply* **2020**, *20*, 984–996, doi:10.2166/ws.2020.021.
42. El-Dessouky, H.T.; Ettouney, H.M. *Fundamentals of Salt Water Desalination*; Elsevier: Amsterdam, The Netherlands, 2002.
43. Lazzaretto, A.; Tsatsaronis, G. SPECO: A systematic and general methodology for calculating efficiencies and costs in thermal systems. *Energy* **2006**, *31*, 1257–1289, doi:10.1016/j.energy.2005.03.011.
44. Bejan, A.; Tsatsaronis, G.; Moran, M. *Thermal Design and Optimization*; John Wiley and Sons, Inc.: New York, NY, USA, 1996.
45. Ehyaei, M.A.; Ahmadi, A.; Rosen, M.A.; Davarpanah, A. Thermodynamic Optimization of a Geothermal Power Plant with a Genetic Algorithm in Two Stages. *Processes* **2020**, *8*, 1277, doi:10.3390/pr8101277.
46. Zeinodini, M.; Aliehyaei, M. Energy, exergy, and economic analysis of a new triple-cycle power generation configuration and selection of the optimal working fluid. *Mech. Ind.* **2019**, *20*, 501, doi:10.1051/meca/2019021.
47. Bellos, E.; Pavlovic, S.; Stefanovic, V.; Tzivanidis, C.; Nakomcic-Smaradgakis, B.B. Parametric analysis and yearly performance of a trigeneration system driven by solar-dish collectors. *Int. J. Energy Res.* **2019**, *43*, 1534–1546, doi:10.1002/er.4380.
48. Tzivanidis, C.; Bellos, E.; Antonopoulos, K.A. Energetic and financial investigation of a stand-alone solar-thermal Organic Rankine Cycle power plant. *Energy Convers. Manag.* **2016**, *126*, 421–433, doi:10.1016/j.enconman.2016.08.033.
49. Nami, H.; Ertesvåg, I.S.; Agromayor, R.; Riboldi, L.; Nord, L.O. Gas turbine exhaust gas heat recovery by organic Rankine cycles (ORC) for offshore combined heat and power applications—Energy and exergy analysis. *Energy* **2018**, *165*, 1060–1071, doi:10.1016/j.energy.2018.10.034.
50. Ehyaei, M.; Ahmadi, A.; Rosen, M.A. Energy, exergy, economic and advanced and extended exergy analyses of a wind turbine. *Energy Convers. Manag.* **2019**, *183*, 369–381, doi:10.1016/j.enconman.2019.01.008.
51. Alizadeh, S.M.; Ghazanfari, A.; Ehyaei, M.A.; Ahmadi, A.; Jamali, D.H.; Nedaei, N.; Davarpanah, A. Investigation the Integration of Heliostat Solar Receiver to Gas and Combined Cycles by Energy, Exergy, and Economic Point of Views. *Appl. Sci.* **2020**, *10*, 5307, doi:10.3390/app10155307.
52. Flinnsci. Sodium Chloride Laboratory Grade 500 g. 2020. Available online: https://www.flinnsci.com/sodium-chloride-laboratory-grade-500-g/s0063/ (accessed on 3 June 2020).
53. Nami, H.; Akrami, E. Analysis of a gas turbine based hybrid system by utilizing energy, exergy and exergoeconomic methodologies for steam, power and hydrogen production. *Energy Convers. Manag.* **2017**, *143*, 326–337, doi:10.1016/j.enconman.2017.04.020.
54. Lee, H.-J.; Yoo, S.-H.; Huh, S.-Y. Economic benefits of introducing LNG-fuelled ships for imported flour in South Korea. *Transp. Res. Part D Transp. Environ.* **2020**, *78*, 102220, doi:10.1016/j.trd.2019.102220.
55. Lecompte, S.; Huisseune, H.; Broek, M.V.D.; De Schampheleire, S.; De Paepe, M. Part load based thermo-economic optimization of the Organic Rankine Cycle (ORC) applied to a combined heat and power (CHP) system. *Appl. Energy* **2013**, *111*, 871–881, doi:10.1016/j.apenergy.2013.06.043.
56. Alshammari, F.; Karvountzis-Kontakiotis, A.; Pesyridis, A.; Usman, M. Expander Technologies for Automotive Engine Organic Rankine Cycle Applications. *Energies* **2018**, *11*, 1905, doi:10.3390/en11071905.
57. Bejan, A.; Tsatsaronis, G.; Moran, M. J. *Thermal Design and Optimization*; John Wiley & Sons: Hoboken, NJ, USA, 1995.
58. Couper, J.R.; Penney, W.R.; Fair, J.R.; Walas, S.M. (Eds.) Chapter 21—Costs of Individual Equipment. In *Chemical Process Equipment*, 2nd ed.; Gulf Professional Publishing: Burlington, VT, USA, 2005; pp. 719–728.
59. Roosen, P.; Uhlenbruck, S.; Lucas, K. Pareto optimization of a combined cycle power system as a decision support tool for trading off investment vs. operating costs. *Int. J. Therm. Sci.* **2003**, *42*, 553–560, doi:10.1016/s1290-0729(03)00021-8.
60. 1000kg/H Steam Boiler Natural Gas/LPG/CNG/LNG Fired Steam Boiler with High Quality, in, 2020.
61. Du, Y.; Xie, L.; Liu, J.; Wang, Y.; Xu, Y.; Wang, S. Multi-objective optimization of reverse osmosis networks by lexicographic optimization and augmented epsilon constraint method. *Desalination* **2014**, *333*, 66–81, doi:10.1016/j.desal.2013.10.028.
62. Ahmadi, A.; Esmaeilion, F.; Esmaeilion, A.; Ehyaei, M.A.; Silveira, J.L. Benefits and Limitations of Waste-to-Energy Conversion in Iran. *Renew. Energy Res. Appl.* **2020**, *1*, 27–45, doi:10.22044/RERA.2019.8666.1007.

63. Marques, R.C. Comparing private and public performance of Portuguese water services. *Hydrol. Res.* **2007**, *10*, 25–42, doi:10.2166/wp.2007.033.
64. Pierobon, L.; Nguyen, T.-V.; Larsen, U.; Haglind, F.; Elmegaard, B. Multi-objective optimization of organic Rankine cycles for waste heat recovery: Application in an offshore platform. *Energy* **2013**, *58*, 538–549, doi:10.1016/j.energy.2013.05.039.
65. Berhane, H.G.; Gonzalo, G.G.; Laureano, J.; Dieter, B. Design of environmentally conscious absorption cooling systems via multi-objective optimization and life cycle assessment. *Appl. Energy* **2009**, *86*, 1712–1722, doi:10.1016/j.apenergy.2008.11.019.
66. Shafer, T. Calculating Inflation Factors for Cost Estimates. In *City of Lincoln Transportation and Utilities Project Delivery*; Public Works: Lincoln, NE, USA, 2021.
67. Alaloul, W.S.; Musarat, M.A.; Liew, M.; Qureshi, A.H.; Maqsoom, A. Investigating the impact of inflation on labour wages in Construction Industry of Malaysia. *Ain Shams Eng. J.* **2021**, doi:10.1016/j.asej.2020.08.036.
68. Edalati, S.; Ameri, M.; Iranmanesh, M.; Tarmahi, H.; Gholampour, M. Technical and economic assessments of grid-connected photovoltaic power plants: Iran case study. *Energy* **2016**, *114*, 923–934, doi:10.1016/j.energy.2016.08.041.
69. Emara, H.I. Nutrient salts, inorganic and organic carbon contents in the waters of the Persian Gulf and the Gulf of Oman. *J. Persian Gulf* **2010**, *1*, 33–44.
70. FILMTEC™ Membranes. How to Evaluate the Active Membrane Area of Seawater Reverse Osmosis Elements. 2015. Available online: dupont.com/content/dam/dupont/amer/us/en/water-solutions/public/documents/en/45-D01504-en.pdf (accessed on 3 June 2020).